ELSEVIER

Thin Solid Films 396 (2001) 183–190

thin solid films

www.elsevier.com/locate/tsf

Thermally- and photo-induced changes in the structure and optical properties of amorphous $As_{40}S_{30}Se_{30}$ films

E. Márquez[a,*], J.M. González-Leal[a], R. Jiménez-Garay[a], M. Vlcek[b]

[a]*Departamento de Física de la Materia Condensada, Facultad de Ciencias, Universidad de Cádiz, 11510 Puerto Real (Cádiz), Spain*
[b]*Department of General and Inorganic Chemistry, Faculty of Chemical Technology, University of Pardubice, 53210 Pardubice, Czech Republic*

Received 24 May 2000; received in revised form 17 April 2001; accepted 19 June 2001

Abstract

Annealing at a temperature near the glass transition temperature and exposure with bandgap light, in air, of thermally-evaporated amorphous $As_{40}S_{30}Se_{30}$ films, were found to be accompanied by structural effects, which, in turn, lead to changes in the refractive index and shifts in the optical absorption edge. Also, indications of photo-oxidation were found after light exposure. An optical characterisation method, based only on the transmission spectra at normal incidence of uniform thin films, has been used to obtain the thicknesses and optical constants corresponding to the virgin, annealed and exposed $As_{40}S_{30}Se_{30}$ samples. The dispersion of the refractive index is discussed in terms of the single-oscillator Wemple–Di Domenico model. The absorption edges are described using both the Urbach rule and the 'non-direct transition' model proposed by Tauc. Regarding the structural transformations that take place in $As_{40}S_{30}Se_{30}$ chalcogenide films when annealed or exposed, the clear decrease and the small shift to higher angle of the intensity profile of the first sharp diffraction peak in the X-ray diffraction pattern, with both treatments, has been interpreted as a diminution of the interstitial volume around the $AsS_{3-n}Se_n$ pyramidal structural units, which form the amorphous network. This significant result is certainly consistent with the decrease of the thickness found for the annealed and illuminated samples.

Keywords: Amorphous materials; Evaporation; Structural properties; Optical properties

1. Introduction

Films of chalcogenide glasses are a subject of systematic research because of the changes in physical and chemical properties which take place in samples after annealing or illumination [1–6]. These thermally- and photo-induced processes offer the possibility of using amorphous chalcogenide semiconductors for high-density information storage, high-resolution display devices and fabrication of diffractive optical elements [7]. In particular, $As_{40}S_{60-x}Se_x$ ternary mixed glasses are attractive candidates for all these technological applications [8–10].

The aim of the present paper is to study the changes in the structure and optical properties of thermally-evaporated amorphous films of chemical composition $As_{40}S_{30}Se_{30}$ (this particular composition being at the middle of the above-mentioned composition line), after annealing at a temperature relatively near the glass transition temperature, T_g, and after illumination with bandgap light, in air. The untreated and treated films have been optically characterised using only their transmission spectra at normal incidence, and employing the very accurate method of the envelope curves suggested by Swanepoel for thin films of uniform thickness [11,12], which has been successfully used by the authors in previous studies [13,14]. The results obtained have been systematically compared with those found in the literature for amorphous layers of the closely related binary stoichiometric compositions $As_{40}S_{60}$ (As_2S_3) and

* Corresponding author. Tel.: +34-956-016318; fax: +34-956-016288.
E-mail address: emilio.marquez@uca.es (E. Márquez).

0040-6090/01/$ - see front matter
PII: S0040-6090(01)01219-6

$As_{40}Se_{60}$ (As_2Se_3) [2]. The lack of data in the literature concerning the optical characterisation of films of ternary chalcogenide glasses confirms the significance of this investigation.

2. Experimental

Films were prepared by vacuum evaporation of the powdered, melt-quenched chalcogenide glassy material, onto glass substrates (microscope slides). The thermal evaporation process was performed inside a coating system (Tesla Corporation, model UP-858), at a pressure of approximately 10^{-5} torr. During the deposition process, the substrates were suitably rotated by means of a planetary rotation system, in order to obtain films of uniform thickness. The deposition rate was ≈ 7 nm s^{-1}, as measured by the dynamic weighing method. This deposition rate results in a composition which is very close to that of the initial bulk material: the composition of the samples was found to be $As_{38.9\pm1.4}S_{31.0\pm0.5}Se_{30.2\pm1.7}$, by means of electron microprobe X-ray analysis (using a scanning electron microscope (SEM) Jeol, model JSM-820). Some as-deposited $As_{40}S_{30}Se_{30}$ layers were annealed at 160°C (the value of T_g is 191°C) for approximately 24 h, under a vacuum of approximately 10^{-3} torr. Other virgin layers were illuminated in air, by a 500 W Hg arc lamp (Oriel, model 6285) through an infrared (IR)-cut filter, providing broadband white light, with a very high ultraviolet (UV) output [15], and with a light intensity of ≈ 40 mW cm^{-2}. It should be emphasised that approximately 3 h of illumination with the Hg lamp, was found to be enough to reach the saturation state.

The lack of crystallinity in the as-evaporated films was verified by X-ray diffraction (XRD) measurements (using a Philips, model PW-1820 diffractometer). After annealing or illumination, the XRD-analysis was also performed in order to study the structural changes occurring during these two treatments. The optical transmission spectra were obtained by a double-beam UV/Vis/NIR spectrophotometer (Perkin-Elmer, model Lambda-19), and the wavelength range analysed was 400–2500 nm. The transmission measurements were made in various parts of the films, scanning the entire sample, and excellent reproducibility of the transmission spectrum was generally achieved. The spectrophotometer was set with suitable slit widths of 0.4 and 1.0 nm, in the UV/Vis spectral region. A surface-profiling stylus instrument (Sloan, model Dektak 3030) was also used to independently measure the film thickness, which was compared with the thickness calculated from the transmission measurements. The thicknesses of the investigated $As_{40}S_{30}Se_{30}$ chalcogenide films were in the range of 800–1400 nm. Furthermore, mass measurements were made by a microbalance (Mettler, model AE200) to check possible changes as a result of both treatments.

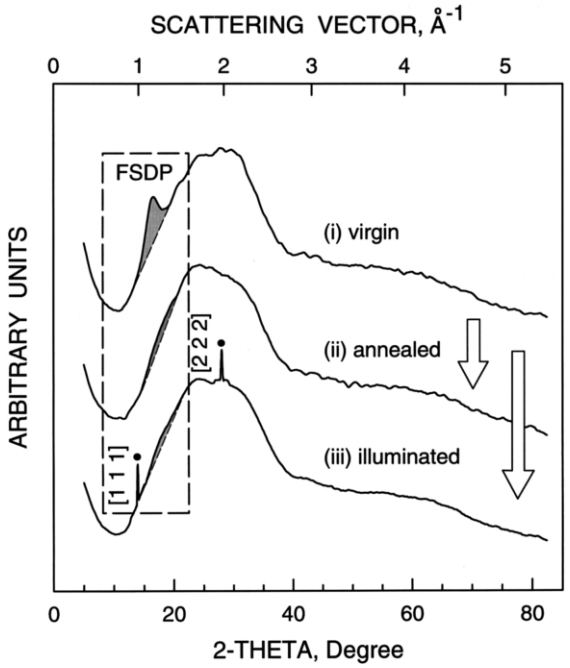

Fig. 1. XRD-patterns (Cu K_α radiation, $\lambda = 1.54$ Å) of the untreated and treated amorphous $As_{40}S_{30}Se_{30}$ films: (i) virgin; (ii) annealed at 160°C; and (iii) exposed to bandgap illumination in air. The data have been smoothed by means of the Savitzsky–Golay filter.

3. Results and discussion

3.1. X-Ray diffraction

Fig. 1 shows the XRD-patterns corresponding to representative as-deposited, annealed and illuminated films. A significant feature of the diffraction data of covalently-bonded amorphous solids, which has long been associated with the presence of medium-range order, is the first sharp diffraction peak (FSDP), occurring at values of the scattering vector $Q(=(4\pi\sin\theta)/\lambda) = 1$–$2$ $Å^{-1}$, depending on the material [2,16,17]. In the present case, this feature appears initially at $2\theta = 16.54°$, or equivalently at $Q = 1.17$ $Å^{-1}$.

Many attempts have been made to explain the origin of the FSDP in glasses. Elliott [16,17] has proposed an explanation in which the FSDP is ascribed to a chemical-order pre-peak (in the concentration–concentration partial structural factor, $S_{cc}(Q)$, in the Bhatia–Thornton formalism [18]), due to the interstitial volume around the cation-centred structural units. This association of the FSDP with correlations involving interstitial voids, plausibly explains the anomalous behaviour of this peak as a function of temperature and pressure.

It can be seen in Fig. 1 that, after both annealing and exposure of the virgin samples, the intensity profile of the FSDP strongly decreases and shifts slightly to higher angle. These experimental results suggest, according to

Elliott's ideas, a thermal- and photo-densification of the amorphous structure, i.e. a clear diminution of the interstitial volume around the $AsS_{3-n}Se_n$ pyramidal structural units, which form the layered network of the $As_{40}S_{60-x}Se_x$ mixed glasses [19]. It is well known [4,20–22] that the as-evaporated amorphous As–S and As–Se films often contain some of the molecular species of which the vapour is composed: mainly, quasi-spherical As_4S_4 or As_4Se_4 molecules. These molecular clusters make difficult the cohesion between the structural layers, increasing the free volume in the material. Virgin films are unstable with respect to annealing or illumination, which lead to the rupture of bonds within the cage-like As_4S_4 or As_4Se_4 molecules [4,20,21]. So, under prolonged annealing or light exposure, the concentration of these molecular species is greatly reduced through polymerisation and cross-linking with the amorphous matrix. Consequently, a more effective interaction between the structural layers, through an increased number of intermolecular chemical bonds, is achieved. Such bonds are of the van der Waals type between As atoms and S or Se atoms. Thus, the structure and mass density of the treated chalcogenide film become virtually identical to that of the corresponding bulk glass. Due to the fact that the As_4S_4 molecule is thermodynamically more stable than the As_4Se_4 entity [20], a higher concentration of the As_4S_4 molecular species is expected in the as-deposited amorphous $As_{40}S_{30}Se_{30}$ films, and, therefore, the observed thermal- and photo-densification phenomena, could basically involve the polymerisation of As_4S_4 molecules, which are more abundant. Lastly, it is important to note that in thermal annealed and illuminated $As_{40}S_{60}$ and $As_{40}Se_{60}$ binary layers, a strong change in the FSDP was previously reported by De Neufville et al. [2].

3.2. Optical properties

3.2.1. Dispersion of the refractive index

The study of the thermally- and photo-induced changes in the optical properties of $As_{40}S_{30}Se_{30}$ chalcogenide films, has been carried out, as already stated, using a method suggested by Swanepoel [11,12] for the case of uniform thin layers, which is based on the upper and lower envelopes, T_+ and T_-, respectively, of the transmission spectrum at normal incidence. Initial values for refractive index, n, corresponding to certain wavelengths, λ_i, for which the envelopes are tangent to the transmission spectrum, were obtained from the following expression

$$n=\sqrt{N+\sqrt{N^2-s^2}} \tag{1a}$$

with s being the refractive index of the substrate, for the wavelengths λ_i, which was independently calculated from the transmission spectrum of the bare substrate (see Ref. [11]), and N given by

$$N=2s\frac{T_+-T_-}{T_+T_-}+\frac{s^2+1}{2} \tag{1b}$$

The top and bottom envelopes were carefully computer-drawn using software created by McClain et al. [23].

A first estimate of the film thickness, d, was obtained using the relationship

$$d=\frac{\lambda_i\lambda_{i+1}}{4(n_{i+1}\lambda_i-n_i\lambda_{i+1})} \tag{2}$$

where n_i and n_{i+1} are the refractive indices for two adjacent tangent points, having wavelengths λ_i and λ_{i+1}, respectively. The above expression is derived from the well-known equation for the appearance of interference fringes

$$2nd=m\lambda \tag{3}$$

with m, the order number, being an integer or half-integer for an upper and lower tangent point, respectively. It should be emphasised that, owing to the optical absorption, this particular equation is not valid at the interference maxima and minima, but at the tangent points referred to (see Ref. [12]). Using Eq. (3) repeatedly, new, more accurate values of the film thickness and refractive index were determined using a procedure which was explained in detail in our previous papers [13,14]. Fig. 2 shows a typical optical transmission spectrum for an as-deposited $As_{40}S_{30}Se_{30}$ film, along with its computer-drawn upper and lower envelopes. It is observed the modulation of the upper envelope T_+ by the transmission spectrum of the bare substrate. This effect is less marked in the case of the lower envelope T_-. It must be noted that the influence of these two modulations on the determination of the optical constants as well as the thickness of the chalcogenide layer, is negligible.

It has been found, using the optical characterisation method outlined above, that the annealing of the virgin samples causes a decrease in the film thickness of 1.9% (from 914 ± 6 (0.7%) nm down to 897 ± 7 (0.8%) nm), which is a sign of a thermal-densification process [6] (a change in the mass of the annealed layer, measured by the microbalance, was not observed). Similarly, the exposure of the as-deposited samples to bandgap light induces a decrease in the thickness, in this particular case, of 1.5% (from 930 ± 9 (1.0%) nm down to 916 ± 8 (0.9%) nm), because, as already mentioned, illumination, as well as annealing, takes the structure of the virgin film closer to the network structure of the corresponding bulk glass [4,21] (in the case of the illuminated layer, a change in the mass was not measured either). It is stressed that in the untreated and treated samples, the thicknesses determined by mechanical measurements with the stylus-based surface profiler, were in excellent

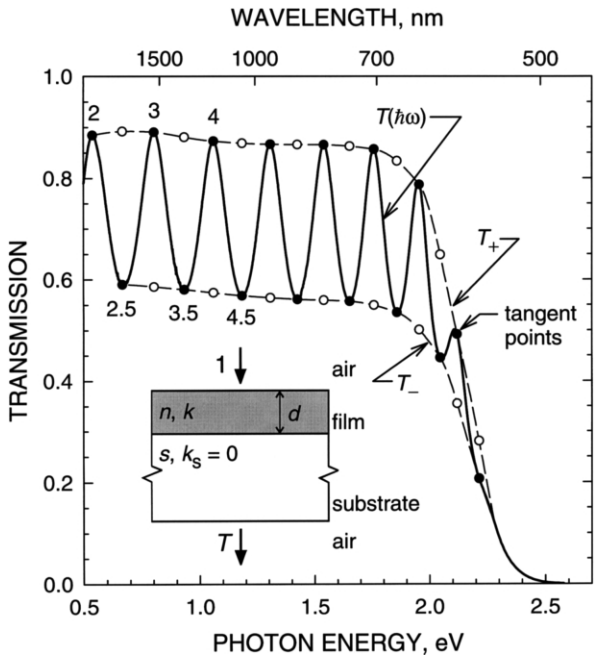

Fig. 2. Transmission as a function of photon energy, $T(\hbar\omega)$, of a 914 ± 6 (0.7%) nm thick, as-evaporated $As_{40}S_{30}Se_{30}$ chalcogenide film; T_+ and T_- are the top and bottom envelope curves, respectively. The order numbers corresponding to some of the upper and lower tangent points, are indicated. The film-on-substrate system is also shown in this figure.

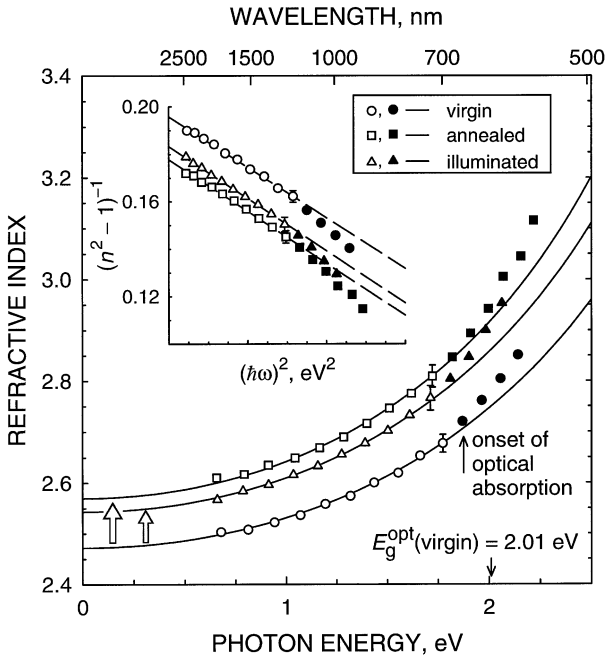

Fig. 3. Refractive index as a function of photon energy, $n(\hbar\omega)$, for the virgin, annealed and exposed $As_{40}S_{30}Se_{30}$ samples. The curves have been drawn from the Wemple–Di Domenico dispersion relationship. In the inset, the plot of the refractive-index factor $(n^2-1)^{-1}$ vs. $(\hbar\omega)^2$.

agreement with those calculated by the optical method (the differences being always less than 2%).

In Fig. 3, the final values of the refractive index are plotted as a function of photon energy. In this figure, it can be seen that n increases both upon annealing and upon illumination. An explanation that could account for this increase is presented below. On the other hand, the dispersion of the refractive index has been analysed in terms of the Wemple–Di Domenico model [24,25], which is based on the single-oscillator formula

$$n^2(\hbar\omega)=1+\frac{E_0E_d}{E_0^2-(\hbar\omega)^2} \quad (4)$$

where E_0 is the oscillator energy and E_d the dispersion energy or oscillator strength. By plotting $(n^2-1)^{-1}$ against $(\hbar\omega)^2$ and fitting a straight line, as shown in the inset of Fig. 3, E_0 and E_d are directly determined from the slope, $(E_0\ E_d)^{-1}$, and the intercept, E_0/E_d, on the vertical axis. However, it must be noted that, due to optical absorption, the experimental variation in the refractive index clearly departs from that given by Eq. (4), when the photon energy approaches the Tauc gap, E_g^{opt}, which will be defined later, when the absorption edge is studied (see Fig. 3) [24,26].

The values of the dispersion parameters E_0 and E_d, as well as the corresponding static refractive index $n(0)$ (the refractive index at $\hbar\omega=0$, $n(0)=\sqrt{1+E_d/E_0}$), for the as-evaporated, annealed and exposed films are listed in Table 1. The oscillator energy E_0 is an 'average' energy gap, and to a good approximation it scales with the optical band gap E_g^{opt}, $E_0\approx2\times E_g^{opt}$, as was found by Tanaka [28] investigating well-annealed As_xS_{100-x} chalcogenide layers. Moreover, the dispersion energy E_d

Table 1
Values of the oscillator energy or Wemple–Di Domenico gap (E_0), dispersion energy or oscillator strength (E_d), static refractive index [$n(0)$], Urbach energy (E_e), Tauc slope ($B^{1/2}$) and optical gap (E_g^{opt}), an alternative option for the optical gap (E_{04}), and the E_0/E_g^{opt} ratio

Sample	E_0 (eV)	E_d (eV)	$n(0)$	E_e (meV)	$B^{1/2}$ ($cm^{-1/2}$ $eV^{-1/2}$)	E_g^{opt} (eV)	E_{04} (eV)	$E0/E_g^{opt}$
Virgin	4.28 ± 0.04	21.88 ± 0.21	2.471 ± 0.002	101 ± 1	772 ± 1	2.01 ± 0.01	2.20 ± 0.01	2.13 ± 0.03
Annealed	3.98 ± 0.02	22.30 ± 0.14	2.569 ± 0.002	91 ± 1	837 ± 2	1.97 ± 0.01	2.14 ± 0.01	2.02 ± 0.02
Illuminated	4.11 ± 0.02	22.47 ± 0.11	2.543 ± 0.001	95 ± 1	801 ± 1	1.95 ± 0.01	2.13 ± 0.01	2.11 ± 0.02

The errors of all these optical parameters have directly been derived from the values of each standard deviation σ_{n-1}, associated with the two straight-line parameters, obtained by the least-squares fit.

obeys a simple empirical relationship [24,25]

$$E_d = \beta\, N_c\, Z_a\, N_e \ \text{(eV)} \quad (5)$$

where N_c is the co-ordination number of the cation nearest-neighbour to the anion, Z_a is the formal chemical valence of the anion, N_e is the effective number of valence electrons per anion, and $\beta = 0.37 \pm 0.04$ eV for covalent, crystalline and amorphous materials.

As a consequence of both annealing and illumination, the oscillator strength, E_d, increases. Assuming $N_e = (40\times 5 + 60\times 6)/60 = 9\ 1/3$ and $Z_a = 2$, and that they should not be changed by either of the two treatments, it seems reasonable to ascribe this trend observed in the values of E_d, to an increase in the effective cation co-ordination number N_c. Furthermore, it is well known that the As_2Ch_3 chalcogenides (Ch being a chalcogen atom) consist of two-dimensional structural layers, in which the As co-ordination number is three. Therefore, the proposed increase in the value of N_c, could certainly be explained in terms of an increase of the van der Waals interaction between these two-dimensional structural layers, as a result of the observed thermal- and photo-contraction phenomena.

On the other hand, the changes found in the static refractive index upon annealing ($\Delta n(0) = +0.098 \pm 0.004$) and illumination ($\Delta n(0) = +0.090 \pm 0.003$) are consistent with those reported for low energies (IR-region) by De Neufville et al. [2], for the particular case of the binary stoichiometric $As_{40}S_{60}$ and $As_{40}Se_{60}$ films ($+0.092 \pm 0.01$ and $+0.107 \pm 0.01$, and $+0.058 \pm 0.01$ and $+0.062 \pm 0.01$, respectively). However, it is worth mentioning that, although it has been found in both $As_{40}S_{60}$ and $As_{40}Se_{60}$ layers that the low-energy refractive index increases slightly more after exposure than after annealing, in the case of the static refractive index of $As_{40}S_{30}Se_{30}$ layers, we have obtained the opposite. It should also be pointed out that the static refractive indices corresponding to either the annealed or exposed film under study, attain values very close to that of the $As_{40}S_{30}Se_{30}$ bulk glass at $\lambda = 5$ μm, 2.59, which is derived by extrapolation from the data recently reported by Sanghera et al. [29].

The relative changes found for $n(0)$, +4.0% after annealing, and +3.7% after illumination, could be related to the increase in the density of the layer, ρ, or equivalently, to the decrease of its thickness, according to the Lorentz–Lorenz equation [27]:

$$\frac{\Delta n(0)}{n(0)} = -\frac{6n^2(0)}{[n^2(0)-1][n^2(0)+2]}\frac{\Delta d}{d} \quad (6)$$

where $\Delta d/d = -\Delta\rho/\rho$. Nevertheless, the relative changes found in the thickness, −1.9% and −1.5%, after annealing and after illumination, respectively, do not account completely for the corresponding increases of $n(0)$. Relative changes in $n(0)$ of +2.2% and +1.7% should be expected from Eq. (6). We believe that the differences with the experimentally-obtained relative changes, could be explained in terms of an increase in the number of heteropolar bonds, which are formed at the expense of homopolar bonds, present in the As_4S_4 and As_4Se_4 molecular clusters contained in the virgin film, giving rise to an increase in the effective polarisability of the material.

3.2.2. Absorption edge

In order to study the thermally- and photo-induced changes in the optical absorption edge of the present samples, the absorbance, x, was obtained from the upper envelope, T_+, by means of the following expression [11,12]

$$x = \frac{E_+ - \sqrt{E_+^2 - (n^2-1)^3(n^2-s^4)}}{(n-1)^3(n-s^2)} \quad (7a)$$

where

$$E_+ = \frac{8n^2 s}{T_+} + (n^2-1)(n^2-s^2) \quad (7b)$$

The n values used in Eqs. (7a) and (7b) have been obtained by extrapolation of Eq. (4) towards the lower wavelengths of the spectral range studied. Once the film thickness and absorbance were known, the equation $x = \exp(-\alpha d)$ was solved to calculate the absorption coefficient, α. The extinction coefficient, k, was then determined from the relationship $k = \alpha\lambda/4\pi$. The dependence of the absorption coefficient on photon energy is displayed in Fig. 4, using a semi-logarithmic scale. As can be seen in this figure, the annealing causes a clear shift of the absorption edge of the as-deposited film to lower energies (i.e. thermal-darkening). Similarly, the exposure to bandgap light leads to a significant red shift of the absorption edge of the virgin layer (i.e. photo-darkening).

In addition, to determine the nature of the electronic optical transitions involved and calculate the optical gap, the spectral dependence of the absorption coefficient was analysed. According to Tauc [30], it is possible to separate three distinct regions in the absorption edge of the amorphous semiconductors: the weak absorption tail, the exponential region and the high absorption region. The weak absorption tail originates from defects and impurities, while the exponential region is strongly related to the characteristic structural randomness of the amorphous materials. Finally, the high absorption region determines the optical energy gap.

In the exponential part of the absorption edge (where $1\ \text{cm}^{-1} \le \alpha \le 10^4\ \text{cm}^{-1}$), the absorption coefficient is governed by the so-called Urbach rule [30,31]

$$\alpha(\hbar\omega) = \alpha_0 \exp\left(\frac{\hbar\omega}{E_e}\right) \quad (8)$$

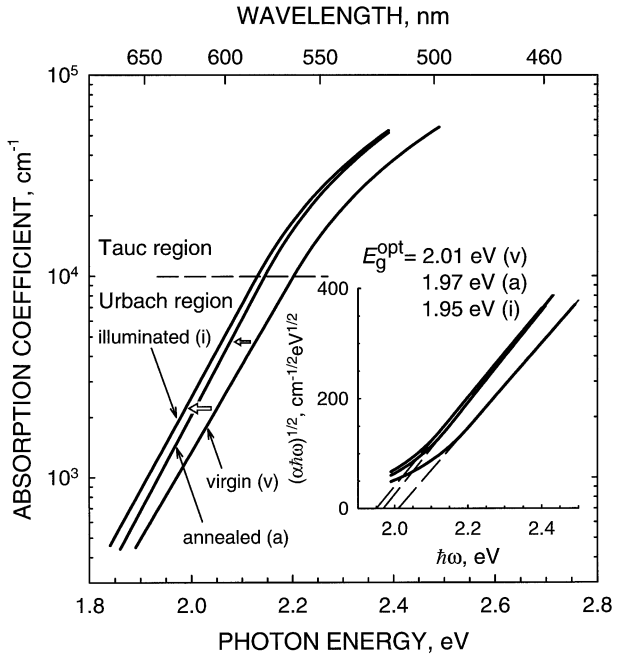

Fig. 4. Changes in the optical absorption edge of a virgin $As_{40}S_{30}Se_{30}$ film, induced by either thermal annealing or bandgap illumination: a red shift takes place in both cases. In the inset, the determination of the optical gap by extrapolation in a $(\alpha\hbar\omega)^{1/2}$ vs. $\hbar\omega$ plot (Tauc's extrapolation).

where the Urbach energy, E_e, characterises the slope of this region. Plotting the dependence of log α on photon energy, as shown in Fig. 4, should give a straight line. The calculated value of E_e, the inverse of the slope of the straight line, gives the width of the tails of the localised states into the gap, at the band edges [32]. The values of E_e found for the virgin, thermal- and photo-darkened $As_{40}S_{30}Se_{30}$ films are all listed in Table 1, and a decrease of the Urbach energy is observed after both treatments.

In the strong absorption region (where $\alpha \geq 10^4$ cm^{-1}), which involves optical transitions between the valence and conduction bands, the absorption coefficient is given, according to the 'non-direct transition' model proposed by Tauc [30], by the following quadratic equation

$$\alpha(\hbar\omega) = B\frac{(\hbar\omega - E_g^{opt})^2}{\hbar\omega} \quad (9)$$

where B is a constant, which depends on the electronic transition probability, and E_g^{opt} is the already introduced Tauc gap, being now formally defined. The values of B and E_g^{opt} can readily be derived from Eq. (9), by plotting $(\alpha\hbar\omega)^{1/2}$ vs. $\hbar\omega$. An excellent fit between the high-energy experimental points and the straight line corresponding to the $(\alpha\hbar\omega)^{1/2}$ vs. $\hbar\omega$ plot, shown in the inset of Fig. 4, indicates that the non-direct transition is certainly the mechanism responsible for the optical absorption in this high-energy spectral region, in the case of the as-deposited, thermal- and photo-darkened $As_{40}S_{30}Se_{30}$ layers.

The values of the Tauc slope and gap, $B^{1/2}$ and E_g^{opt}, respectively, as well as the alternative optical gap, E_{04}, which represents the energy at which the absorption coefficient reaches the value of 10^4 cm^{-1}, for the three representative samples, are presented in Table 1. The change found in the optical gap E_{04} after annealing was $\Delta E_{04} = -0.06$ eV ($\Delta E_g^{opt} = -0.04$ eV), while those reported by De Neufville et al. [2], ΔE_{04} ($As_{40}S_{60}$) and ΔE_{04} ($As_{40}Se_{60}$), were both -0.05 eV. In addition, the change in E_{04} upon illumination was $\Delta E_{04} = -0.07$ eV ($\Delta E_g^{opt} = -0.06$ eV), and those found in Ref. [2] were ΔE_{04} ($As_{40}S_{60}$) $= -0.07$ eV and ΔE_{04} ($As_{40}Se_{60}$) $= -0.06$ eV. The decrease of both gaps is related to the lower energy of the heteropolar bonds, As–S (379.5 kJ mol^{-1}) and As–Se (96 kJ mol^{-1}), compared to the energy of the homopolar bonds, As–As (382.0 kJ mol^{-1}), S–S (425.3 kJ mol^{-1}) and Se–Se (332.6 kJ mol^{-1}), present in the As_4S_4 and As_4Se_4 molecular units embedded in the as-deposited sample. Furthermore, one can conclude from the results listed in Table 1, that the values of the gaps E_0 and E_g^{opt} satisfy the already introduced relationship $E_0 \approx 2 \times E_g^{opt}$. Last but not least, it is important to mention that, according to Zanatta and Chambouleyron [33], the increase found in the Tauc slope after both treatments, is coherent with the corresponding decrease of the Urbach energy.

3.3. Photo-oxidation process

It is important to mention that, as in the previously reported data on exposed $As_{40}S_{60}$ and $As_{40}Se_{60}$ binary chalcogenide layers [1,5], a phase separation, leading to the formation of a new phase of As_2O_3 (arsenolite) on the surface of the $As_{40}S_{30}Se_{30}$ films, has been found. Thus, the XRD-pattern of the representative exposed $As_{40}S_{30}Se_{30}$ film (see Fig. 1) shows two Bragg peaks at $2\theta = 14.02°$ and 28.04° [34]. This surface effect is closely related to the strong optical absorption for high photon energies, that the amorphous chalcogenide layers generally exhibit (see Fig. 4). Moreover, it should be taken into account that the spectral irradiance curve of the Hg arc lamp used in this work to illuminate the virgin samples, shows very high output peaks in the region approximately 300–450 nm (corresponding to photon energies of approximately 4.1–2.8 eV) [15]. Therefore, a considerable part of the radiation emitted by the Hg lamp (mainly, the UV part) does not penetrate into the chalcogenide layer. This is the cause of a partial photo-degradation of the film at its surface.

As light exposure has been carried out in air, both photo-oxidation and photo-hydrolysis could take place (because of the presence of both oxygen and water vapor), which would result in the appearance of small,

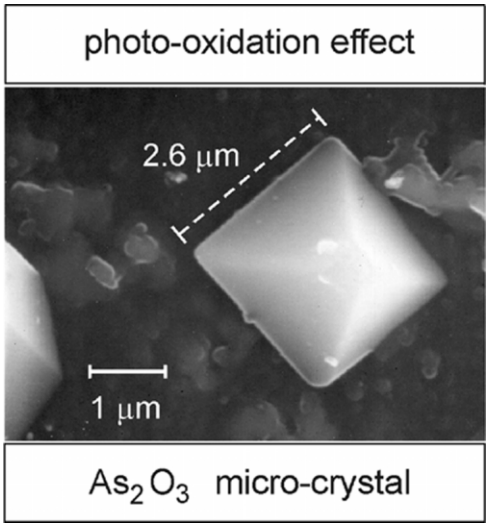

Fig. 5. SEM image of the surface of a representative $As_{40}S_{30}Se_{30}$ sample, after it was exposed to UV-light for around three hours, at ambient conditions. A micro-crystal of arsenolite is clearly displayed in this figure.

but recognizable arsenic trioxide micro-crystals [1,5]. The surface morphology of the illuminated samples was carefully observed under the SEM, in order to identify these As_2O_3 micro-crystals (see Fig. 5). Owing to the very low concentration of them on the surface of the samples, they should not significantly influence the present optical transmission measurements nor, consequently, all the results derived from them. Finally, it has to be pointed out that no measurable compositional change was found in the exposed layers, by energy-dispersive spectroscopy.

4. Conclusions

Thermally-evaporated amorphous $As_{40}S_{30}Se_{30}$ films undergo structural transformations when annealed at a temperature near T_g (i.e. a thermo-structural transformation), and when exposed to bandgap illumination, with a Hg arc lamp, in air (i.e. a photo-structural transformation). The clear decrease and the small shift to higher angle of the FSDP in the XRD-pattern, with both treatments, has been interpreted as a diminution of the interstitial volume around the $AsS_{3-n}Se_n$ pyramidal structural units, through the polymerisation of the As_4S_4 and, in a smaller degree, As_4Se_4 molecules, leading to a more nearly cross-linked structure. This significant result is certainly consistent with the decrease of the thickness found for the samples, whether annealed or illuminated. Also, indications of a photo-oxidation process on the surface of the films have been found: arsenic trioxide micro-crystals were unequivocally identified visually, by SEM, and structurally, by XRD-measurements. Nevertheless, the influence of these micro-crystals on the optical transmission measurements is negligible due to the very low observed concentration of them.

Changes in the optical properties of the virgin films after annealing, as well as after bandgap illumination, have systematically been studied in this work. In particular, the refractive indices of the as-evaporated layers increase with either of the two treatments. Another finding is the red shift of the optical absorption edge of the as-deposited sample, as a result of both annealing (a thermal-darkening process has taken place), and light exposure (in other words, a photo-darkening effect).

Acknowledgements

The authors are grateful to Dr P.J.S. Ewen (Department of Electronics and Electrical Engineering, University of Edinburgh, UK) and Dr R. Prieto-Alcón (Departamento de Física de la Materia Condensada, Universidad de Cádiz, Spain) for the critical reading of the paper. This work has been supported by the CICYT (Spain), under the MAT98-0791 project.

References

[1] J.S. Berkes, S.W. Ing, W.J. Hillegas, J. Appl. Phys. 42 (1971) 4908.
[2] J.P. De Neufville, S.C. Moss, S.R. Ovshinsky, J. Non-Cryst. Solids 13 (1973/74) 191.
[3] S.R. Elliott, J. Non-Cryst. Solids 81 (1986) 71.
[4] G. Pfeiffer, M.A. Paesler, S.C. Agarwal, J. Non-Cryst. Solids 130 (1991) 111.
[5] J. Dikova, N. Starbov, K. Starbova, J. Non-Cryst. Solids 167 (1994) 50.
[6] L. Tichý, A. Vidourek, P. Nagels, R. Callaerts, H. Tichá, Opt. Mater. 10 (1998) 117.
[7] S.R. Ovshinsky, H. Fritzsche, IEEE Trans. Electron. 20 (1973) 91.
[8] A.V. Stronski, P.F. Romanenko, I.I. Robur, I.Z. Indutnyi, P.E. Shepeljavi, S.A. Kostyukevich, J. Inf. Rec. Mats. 20 (1993) 541.
[9] I.Z. Indutnyi, P.E. Shepeljavi, P.F. Romanenko, I.I. Robur, A.V. Stronski, in: V.V. Petrov, S.V. Svechnikov (Eds.), International Conference on Optical Storage, Imaging and Transmission of Information, Kiev, Ukraine, 14–16 May 1996, SPIE Proceedings 3055 (1997) 50.
[10] A.V. Stronski, M. Vlcek, A. Sklenar, P.E. Shepeljavi, S.A. Kostyukevich, T. Wagner, J. Non-Cryst. Solids 266–269 (2000) 973.
[11] R. Swanepoel, J. Phys. E: Sci. Instrum. 16 (1983) 1214.
[12] R. Swanepoel, J. Phys. E.: Sci. Instrum. 17 (1984) 896.
[13] E. Márquez, J.B. Ramirez-Malo, P. Villares, R. Jiménez-Garay, P.J. Ewen, A.E. Owen, J. Phys. D: Appl. Phys. 25 (1992) 535.
[14] J.B. Ramírez-Malo, E. Márquez, P. Villares, R. Jiménez-Garay, Mater. Lett. 17 (1993) 327.
[15] Oriel Catalog, Light Sources, Monochromators, Spectrographs, Detectors and Fiber Optics, vol. II, 1994, pp. 1–42.
[16] S.R. Elliott, Nature 354 (1991) 445.
[17] S.R. Elliott, Phys. Rev. Lett. 67 (1991) 711.
[18] A.B. Bhatia, D.E. Thornton, Phys. Rev. B 2 (1970) 3004.
[19] J.A. Freitas, U. Strom, D.J. Treacy, J. Non-Cryst. Solids 59&60 (1983) 875.

[20] S.R. Elliott, in: J. Zarzycki (Ed.), Materials Science and Technology, vol. 9, VCH, New York, 1991, p. 375.
[21] A.E. Owen, P.J.S. Ewen, in: M. Cable, J.M. Parker (Eds.), High-Performance Glasses, Blackie, London, 1991, p. 287.
[22] K.K. Shvarts, J.A. Teteris, I.P. Manika, M.J. Reinfelde, V.I. Gerbreder, J. Non-Cryst. Solids 90 (1987) 509.
[23] M. McClain, A. Feldman, D. Kahaner, X. Ying, J. Comput. Phys. 5 (1991) 45.
[24] S.H. Wemple, M. Di Domenico, Phys. Rev. B 3 (1971) 1338.
[25] S.H. Wemple, Phys. Rev. B 7 (1973) 3767.
[26] I. Solomon, M.P. Schmidt, C. Sénémaud, M. Driss Khodja, Phys. Rev. B 38 (1988) 13263.
[27] S. Rajagopalan, K.S. Harshavardhan, L.K. Malhotra, K.L. Chopra, J. Non-Cryst. Solids 50 (1982) 29.
[28] Ke. Tanaka, Thin Solid Films 66 (1980) 271.
[29] J.S. Sanghera, V.Q. Nguyen, I.D. Aggarwal, J. Am. Ceram. Soc. 79 (1996) 1324.
[30] J. Tauc, in: J. Tauc (Ed.), Amorphous and Liquid Semiconductors, Plenum, New York, 1974, p. 171.
[31] F. Urbach, Phys. Rev. 92 (1953) 1324.
[32] M.M. Hafiz, A.H. Moharram, A.A. Abu-Sehly, Appl. Phys. A 66 (1998) 217.
[33] A.R. Zanatta, I. Chambouleyron, Phys. Rev. B 53 (1996) 3833.
[34] Powder Diffraction File, Joint Committee on Powder Diffraction Standards, ASTM, Philadelphia, PA, 1996, Card 36–1490.